

# Dripping Channel Based Liquid Triboelectric Nanogenerators for Energy Harvesting and Sensing

Wei Zhong,<sup>#</sup> Liang Xu,<sup>#</sup> Fei Zhan, Haiming Wang, Fan Wang, and Zhong Lin Wang\*



Cite This: <https://dx.doi.org/10.1021/acsnano.0c04413>



Read Online

ACCESS |



Metrics & More



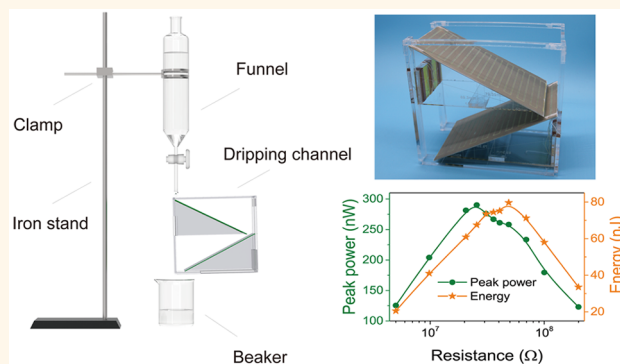
Article Recommendations



Supporting Information

**ABSTRACT:** Dripping liquid is one of the most common practices in chemistry, but one rarely thinks that the contact of liquid with air could introduce charges in the liquid, which may affect the chemical reaction. Here, we propose a functional dripping channel based on a liquid triboelectric nanogenerator (L-TENG) to effectively harvest energy from liquid droplets and sense their motion. The L-TENG is a hybrid of a grating-electrode L-TENG and a single-electrode L-TENG, which are for energy harvesting and sensing, respectively. When dripping from a funnel, the energy of the droplets can be successively harvested and stored. Meanwhile, the single-electrode L-TENG can identify the time interval for the liquid flow and the number of droplets, providing information on the chemical process. The device with enhanced energy harvesting and sensing functions should have great application prospects in intelligent laboratory systems and can also contribute to the optimization of the L-TENGs for harvesting liquid droplet energy.

**KEYWORDS:** triboelectric nanogenerator, droplet, dripping channel, energy harvesting, intelligent chemistry



In the chemical reaction system, the injection of reactants and the collection of products are usually accompanied by the dripping of liquid. Traditionally, droplets pass the air between the nozzle and the target container, which acts as a dripping channel without other functions. With the advent of the intelligent era, intelligent laboratory systems are proposed where chemical reactions can be better sensed and controlled.<sup>1</sup> Dripping channels with more functions can contribute greatly to the development of such systems. The invention of triboelectric nanogenerators (TENGs, also called a Wang generator), which can derive their origin from Maxwell's displacement current, provides opportunities for developing functional dripping channels.<sup>2,3</sup> The basic working principle of the triboelectric nanogenerator is based on the coupling of triboelectrification and electrostatic induction.<sup>4,5</sup> It has the characteristics of lightweight and variable structures and is particularly efficient in converting low-frequency and low-amplitude mechanical energy into electricity.<sup>6–8</sup> Since the invention of triboelectric nanogenerators, there has been a lot of research on the electrification of liquid and solid interfaces.<sup>9</sup> At present, it turns out that electrification in liquid–solid contact can be mainly attributed to electron transfer.<sup>10,11</sup> In 2013, energy harvesting based on liquid–solid contact was realized successfully.<sup>12</sup> Subsequently, liquid–solid electrification was

used to harvest and sense fluid energy, to harvest wave energy, and to detect the draft of ships.<sup>13–21</sup> So far, the application of liquid–solid electrification in chemical systems has only appeared in microfluidic chemistry. In combination with the micrototal analysis system, a microfluidic channel based on a triboelectric nanogenerator is proposed to harvest energy from fluid and sense the parameters of the fluid.<sup>22–24</sup> No functional devices based on triboelectric nanogenerators have been embedded in macrofluid chemical systems.<sup>9</sup>

Here, we propose a dripping channel based liquid triboelectric nanogenerator (L-TENG) for energy harvesting and sensing of droplets, enabling intelligent chemical systems. The L-TENG adopts a hybrid structure of a grating-electrode L-TENG and a single-electrode L-TENG, which are for energy harvesting and sensing, respectively. The grating-electrode structure can improve the energy harvesting performance,<sup>25–29</sup> and a folded

Received: May 27, 2020

Accepted: July 20, 2020

Published: July 20, 2020

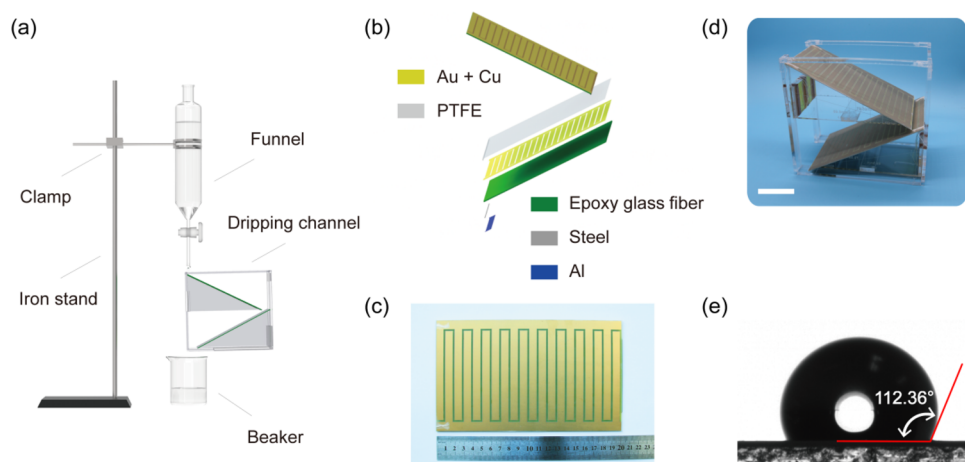


**Figure 1.** Design of the dripping channel and structure of the L-TENG device. (a) Schematic of the dripping channel. (b) Structure of the L-TENG. (c) Photograph of the electrode arrangement. (d) Photograph of the fabricated L-TENG device (Scale bar: 5 cm). (e) Contact angle of the pristine PTFE.

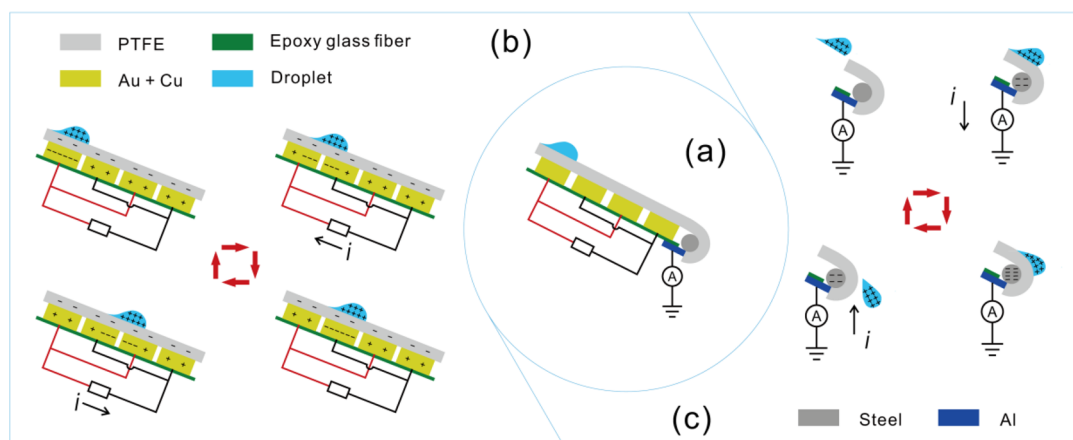


**Figure 2.** Working mechanism of the L-TENG. (a) Schematic of the total structure with a grating-electrode L-TENG and a single-electrode L-TENG. (b) Working principle of the grating-electrode L-TENG for harvesting the energy of a droplet. (c) Working principle of the single-electrode L-TENG for sensing a droplet.

structure is designed to reduce the volume for increasing the output density.<sup>30–35</sup> Compared to the unfolded structure, the folded structure with three segments shows an enhancement of 123.06% in maximum peak power density and 141.18% in maximum energy density. A typical setup in chemistry is demonstrated. When dripping from a funnel, the energy of droplets can be successively harvested and stored. Meanwhile, the single-electrode L-TENG can identify the time interval, the number of droplets, and the total duration of the droplets, providing information on the chemical process. The device with enhanced energy harvesting and sensing functions should have a great application prospect in intelligent laboratory systems and can also contribute to the optimization of the L-TENGs for harvesting droplet energy.

## RESULTS AND DISCUSSION

The dripping channel in a typical setup for chemical reactions is shown in Figure 1a. There are three parts in the setup: the funnel used as the source of the droplets, the beaker used as the receiver of the falling droplets, and the iron stand and clamp for fixing the funnel at a certain height. This setup is widely adopted in chemical experiments to add reactant A from a funnel to another reactant B in a beaker. The energy of the droplets can be

harvested in the dripping channel based L-TENG for intelligent chemistry or other applications. A schematic explosive view of the major part of the L-TENG is shown in Figure 1b. A folded slope structure of the electrode panels is designed in the L-TENG for enhancing performance. The electrode panel contains three parts, which are an epoxy glass fiber substrate, a Au + Cu grating electrode layer, and a polytetrafluoroethylene (PTFE) film. A steel rod is placed at the end of the electrode panel. A photograph of the electrode panel is shown in Figure 1c with dimensions of 12 cm × 20 cm. The fabricated L-TENG device is shown in Figure 1d. The contact angle of the pristine PTFE used here is about 112.36°, as shown in Figure 1e. The microstructure on the surface of the PTFE film is shown in Figure S1.

The L-TENG is designed as a hybrid of a grating-electrode L-TENG and a single-electrode L-TENG, as shown in Figure 2a. The grating-electrode L-TENG is based on the freestanding-triboelectric-layer mode (Figure 2b). The charges on a droplet may come from two sources. Because PTFE has a strong affinity to electrons, the droplet will be positively charged when sliding on the surface of PTFE owing to electron transfer from water to PTFE due to contact electrification. On the other hand, friction between air and a droplet can also contribute to the positive

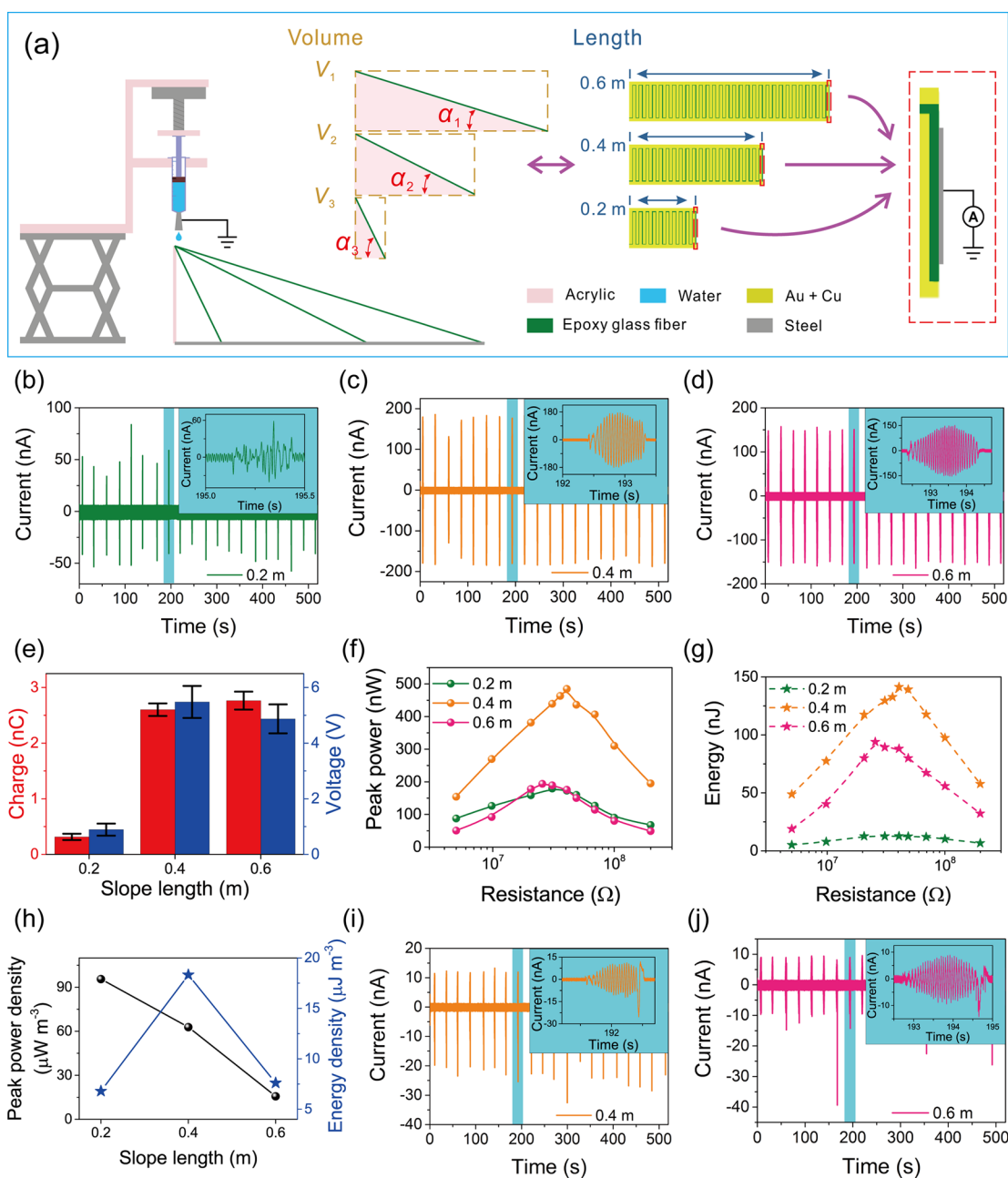


**Figure 3.** Basic characterization of the L-TENG tested with a motor. (a) Schematic of the experimental setup and unfolded electrode panels with three different lengths. (b–d) Short-circuit current of the unfolded grating-electrode L-TENGs with 0.2 m (b), 0.4 m (c), and 0.6 m (d) electrode panels, respectively. (e) Transferred charges and open-circuit voltage for different unfolded grating-electrode L-TENGs. (f, g) Peak power (f) and energy (g) of the unfolded grating-electrode L-TENGs. (h) Maximum peak power density and energy density of the unfolded grating-electrode L-TENGs. (i, j) Short-circuit current of the single-electrode L-TENGs with 0.4 m (i) and 0.6 m (j) electrode panels, respectively.

electrification of the droplet. The charges on the droplet will induce negative charges in the electrodes underneath the PTFE, which will follow the sliding of the charged droplet and transfer between the pair of grating electrodes on the electrode panel. Because the grating electrodes are arranged in an interdigital way, the sliding droplet can produce alternate current peaks in the external circuit. The single-electrode L-TENG is used for sensing, which is based on the steel rod grounded through an Al sheet. As shown in Figure 2c, the droplet is positively charged as it glides over the PTFE film. When the charged droplet approaches the steel rod, electrons will be attracted to the rod from the ground. When the droplet leaves the end of the

electrode panel, the electrons will flow back to the ground. In such a way, an alternate current signal will be generated in the ground circuit.

In order to characterize the basic performance of the L-TENG, single electrode panels without folding were tested first. A syringe pushed by a motor was used to generate droplets under precise control. The vertical distance between the outlet of the syringe and the electrode panel was 1.5 cm. Pure water with a resistivity of  $18.2 \text{ M}\Omega\text{-cm}$  was adopted for the droplet, and the volume of the water droplet produced by the motor is  $99 \mu\text{L}$ . The detailed experimental setup is shown in Figure 3a. Unfolded electrode panels of three different lengths (0.2 m, 0.4

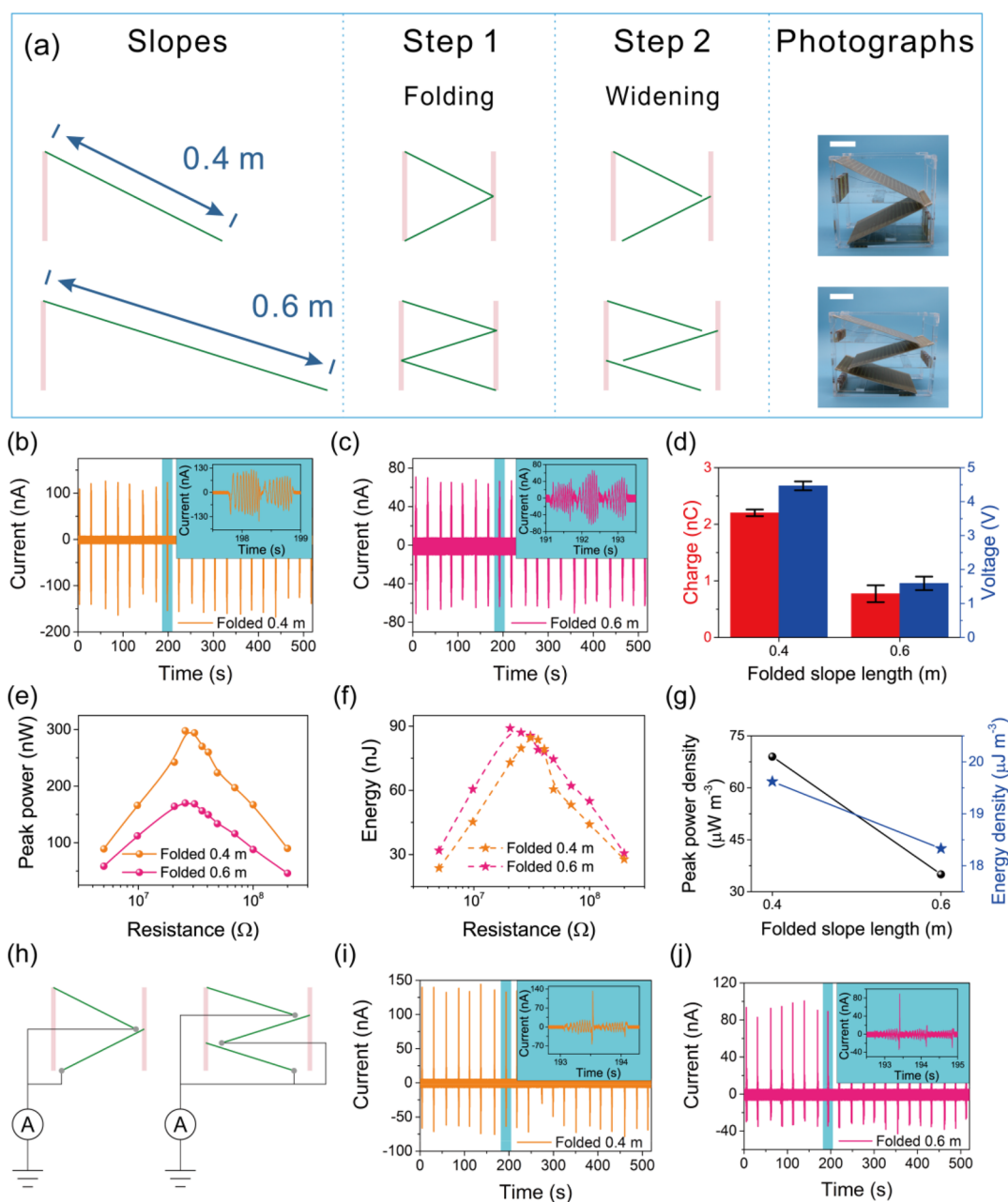


**Figure 4.** Basic characterization of the L-TENG tested with a motor. (a) Folding principle and device photographs (Scale bar: 5 cm). (b, c) Short-circuit current for 0.4 m (b) and 0.6 m (c) folded grating-electrode L-TENGs, respectively. (d) Transferred charges and open-circuit voltage for different folded grating-electrode L-TENGs. (e, f) Peak power (e) and energy (f) of folded grating-electrode L-TENGs. (g) Maximum peak power density and energy density of folded grating-electrode L-TENGs. (h) Measuring circuit for single-electrode L-TENGs. (i, j) Short-circuit current of single-electrode L-TENGs in 0.4 m (i) and 0.6 m (j) L-TENGs, respectively.

m, and 0.6 m) were characterized in the experiment. The three electrode panels were fixed at the same height of 18 cm to form slopes with different inclination angles. The volumes of the cuboids occupied by the three slopes are noted as  $V_1$ ,  $V_2$ , and  $V_3$ , respectively. For each length, the outputs of the grating-electrode L-TENG and the single-electrode L-TENG were measured.

The short-circuit currents of the grating-electrode L-TENGs with the three unfolded electrode panels are shown in Figure 3b–d. The inset figures present the enlarged output curves of the eighth water droplet, which show current outputs of 58.85 nA, 176.84 nA, and 151.08 nA, respectively. The current with the 0.4 m electrode panel is the maximum, and the current in the

0.2 m case is the minimum. The transferred charges and voltage of the grating-electrode L-TENGs were also studied (Figure 3e). The peak-to-peak values of the transferred charges of the three cases are 0.32 nC, 2.6 nC, and 2.76 nC, respectively (details are shown in Figure S2). The peak-to-peak voltages are 0.89 V, 5.48 V, and 4.87 V, respectively (details are shown in Figure S2). The cases with 0.4 and 0.6 m lengths are superior to the 0.2 m case in peak-to-peak transferred charges and voltage. To compare the performance of the three generators in more detail, the peak power and energy were tested. As shown in Figure 3f, the maximum peak power for the 0.4 m case is much larger than for the other two cases, achieving 484.98 nW with a matched resistance of 40.7 M $\Omega$ . The maximum peak powers of the 0.2 m

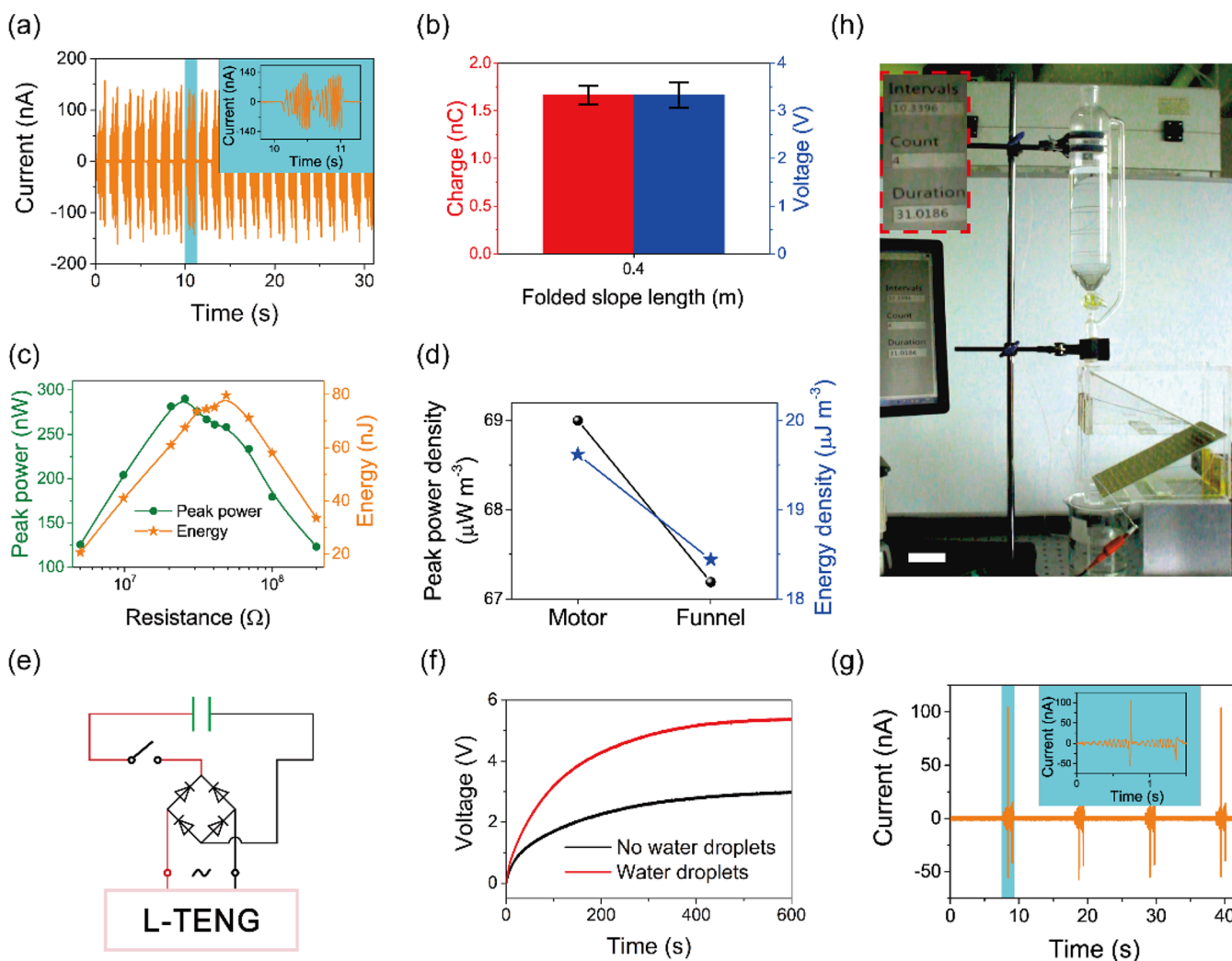


**Figure 5.** Application demonstration of a 0.4 m L-TENG with a dripping funnel. (a) Short-circuit current for the 0.4 m folded grating-electrode L-TENG. (b) Transferred charges and open-circuit voltage for the 0.4 m folded grating-electrode L-TENG. (c) Peak power and energy of the 0.4 m folded grating-electrode L-TENG. (d) Maximum peak power density and energy density of the 0.4 m folded grating-electrode L-TENG with different drives. (e) Rectification circuit diagram for the folded grating-electrode L-TENG to charge a capacitor. (f) Charging performance of the 0.4 m folded grating-electrode L-TENG to a capacitor of 1  $\mu\text{F}$ . (g) Short-circuit current of the single-electrode L-TENGs in the 0.4 m L-TENG. (h) Photograph of the experimental setup for sensing water droplets (scale bar: 5 cm).

and the 0.6 m cases are 179.65 nW and 194.03 nW with matched resistances of 30.9 M $\Omega$  and 25.6 M $\Omega$ , respectively. The peak power is calculated according to the following equation:

$$P_{\text{peak}} = I_{\text{peak}}^2 R \quad (1)$$

where  $R$  is the load resistance and  $I_{\text{peak}}$  is the peak value of the current. The maximum harvested energies during sliding of a single droplet for the three cases are 12.76 nJ, 141.41 nJ, and 93.99 nJ, respectively, as shown in Figure 3g. The energy for a single droplet is calculated according to the following equation:

$$E = \frac{\int_0^{T_E} I^2 R dt}{20} \quad (2)$$

where  $T_E$  is the time span of dripping 20 consecutive droplets. The 0.4 m case has the highest energy output, while the 0.2 m case has the lowest. It is necessary to calculate the output density of the three cases because of their different occupied volumes. As shown in Figure 3h, the maximum peak power densities of the 0.2 m, 0.4 m, and 0.6 m cases are 95.56  $\mu\text{W m}^{-3}$ , 62.82  $\mu\text{W m}^{-3}$ ,

and 15.7  $\mu\text{W m}^{-3}$ , respectively. The 0.2 m case has the maximum peak power density, and the 0.6 m case is the smallest. The maximum energy densities of the three cases are 6.79  $\mu\text{J m}^{-3}$ , 18.32  $\mu\text{J m}^{-3}$ , and 7.6  $\mu\text{J m}^{-3}$ , respectively. The 0.4 m case has the largest energy density, followed by the 0.6 m case, and the 0.2 m case has the smallest value, as shown in Figure 3h. The 0.4 m case with middle length and inclination angle should be more preferable than the other two, which can provide some clues for optimizing similar devices based on droplets.

The device can not only harvest the energy of water droplets but also sense their motion, based on the single-electrode L-TENG. The single-electrode L-TENG is grounded through a current meter when the grating-electrode L-TENG is connected with a matched resistor. In this way, the single-electrode L-TENG can be used to sense the water droplets while harvesting the energy of the droplets with the grating-electrode L-TENG. As shown in the insets of Figure 3i,j, the single-electrode L-TENG in the 0.4 m case has a maximum current of 25.41 nA, and the 0.6 m case has a maximum current of 14.17 nA. The largest peak can be used to identify a single droplet for counting.

In order to increase the output density of the L-TENG, a folded structure is designed to reduce the size of the device. As shown in Figure 4a, folding the L-TENG can effectively save the volume while maintaining the inclination angle. The 0.4 and 0.6 m electrode panels are folded into two and three segments, respectively. The electrode connections among the segments are shown in Figure S3. In order to allow the droplets to slide down along the folded trajectory, the folded structure is widened to introduce a vertical gap of about 10.78 mm between adjacent segments. The photographs of the L-TENGs with a folded structure corresponding to 0.4 and 0.6 m cases are shown in Figure 4a. The short-circuit current of the folded grating-electrode L-TENG is shown in Figure 4b,c, with the output of the eighth water droplet presented in the insets. For the folded 0.4 m case, the peak current in the inset is about 122.88 nA, and the value for the 0.6 m case is 66.29 nA, and both are smaller than the unfolded cases. The peak-to-peak transferred charges and voltage are shown in Figure 4d. The transferred charges of the grating-electrode L-TENGs for the folded 0.4 and 0.6 m cases are 2.2 nC and 0.77 nC, respectively (details are shown in Figure S4). The peak-to-peak open-circuit voltages of the grating-electrode L-TENGs for the folded 0.4 and 0.6 m cases are 4.46 and 1.59 V, respectively (details are shown in Figure S4). The peak power and energy are shown in Figure 4e,f. The maximum peak power values of folded 0.4 and 0.6 m cases are 298.05 nW and 170.21 nW, respectively. The maximum harvested energy values of the two cases are 84.75 nJ and 89.06 nJ, respectively. The maximum peak power of the folded 0.4 m case is larger than that of the folded 0.6 m case, but the harvested energy is a little smaller. The output densities of the folded 0.4 and 0.6 m cases are also calculated, as shown in Figure 4g. The maximum peak power densities of the folded 0.4 and 0.6 m cases are  $69 \mu\text{W m}^{-3}$  and  $35.02 \mu\text{W m}^{-3}$ , respectively. The maximum energy densities of the two cases are  $19.62 \mu\text{J m}^{-3}$  and  $18.33 \mu\text{J m}^{-3}$ , respectively. The maximum output density of the folded 0.4 m case is larger than that of the folded 0.6 m case.

Compared to the unfolded cases, although there is energy loss at the folding joint, the folded structure has the advantages of smaller volume and higher space utilization, and the output density can be greatly improved. The maximum peak power density of the folded 0.4 m case is increased by 9.84% compared with the unfolded 0.4 m case, and the maximum energy density of the folded 0.4 m case is increased by 7.1%. The maximum peak power density of the folded 0.6 m case is increased by 123.06% compared with the unfolded 0.6 m case, and the maximum energy density of the folded 0.6 m case is increased by 141.18%. Therefore, through the folding design of the structure, the droplet energy can be harvested more efficiently, which can also be applied to similar devices.

The single-electrode L-TENG in the structure for sensing was also tested. Measuring the circuit for the single-electrode L-TENG is shown in Figure 4h. At the end of each segment, a single-electrode L-TENG is installed. Thus, there are two single-electrode L-TENGs in the folded 0.4 m case and three in the folded 0.6 m case, which are connected in parallel. The maximum short-circuit current of the single-electrode L-TENG in the folded 0.4 m case can reach around 132.8 nA, as shown in the inset of Figure 4i, and the value for the folded 0.6 m case is around 89.23 nA, as shown in the inset of Figure 4j. The signal can be used for identifying the falling of one droplet.

In order to use the L-TENG as a dripping channel for intelligent chemistry in practical scenarios, a funnel dripping experiment is demonstrated. The 0.4 m L-TENG, which showed

excellent output performance in the motor test, was used for the experiment. The vertical distance between the outlet of the funnel and the electrode panel of the L-TENG was 1.5 cm, which was the same as the motor test. The short-circuit current of the grating-electrode L-TENG in the L-TENG is shown in Figure 5a, and the inset is the output of the eighth droplet, which presents a peak value of 140.45 nA. The peak-to-peak value of transferred charges and open-circuit voltage of the grating-electrode L-TENG are 1.67 nC and 3.33 V, respectively (Figure 5b) (details are shown in Figure S5). The peak power and energy of the grating-electrode L-TENG were also investigated, as shown in Figure 5c. The maximum peak power of the device is 290.25 nW with a matched resistance of 25.6 M $\Omega$ , and the maximum energy is 79.67 nJ. The output density of the device is calculated, as shown in Figure 5d. The maximum peak power density of the device is  $67.19 \mu\text{W m}^{-3}$ , and the maximum energy density of the device is  $18.44 \mu\text{J m}^{-3}$ , which are very close to the output density in the motor test. The results show that the L-TENG has good output stability and energy harvesting applicability in practical scenarios. The harvested energy can also be stored in a capacitor to drive low-power devices. A 1  $\mu\text{F}$  capacitor was connected to the 0.4 m L-TENG for testing the charging performance. The rectification circuit diagram for the L-TENG to charge a capacitor is shown in Figure 5e. The capacitor can be charged to 2.98 V in 600 s without water droplets (Figure 5f). This could be attributed to the electromagnetic waves in the space, which can cause fluctuations of electrical potential between metal electrodes, and charge a capacitor via rectification.<sup>36</sup> When droplets were applied, a voltage of 5.39 V could be achieved in 600 s (Figure 5f). The liquid level in the funnel was between 400 and 500 mL in the experiment, and the droplet size was about 99  $\mu\text{L}$ .

The short-circuit current of the single-electrode L-TENG for the first water droplet is 104.26 nA, as shown in Figure 5g. Figure 5h illustrates the experimental setup for sensing water droplets. Experiments for Figure 5g,h use droplets of 90  $\mu\text{L}$ . The process of droplets dripping from the funnel through the dripping channel is shown in Video S1, and Video S2 demonstrates the sensing process. As shown in the video, the droplet interval, the count of droplets, and the total duration of dripping can be obtained by the dripping channel (Time unit: s). The dripping operation is indispensable in chemical experiments. Based on the dripping channel, plenty of information on the chemical experiments can be obtained automatically, which can show the degree of the dripping and help to estimate the progress of the chemical reaction. Although only water is used here for producing the droplet, other liquids in chemistry are also applicable due to the generality of the triboelectrification phenomenon. The dripping channel based L-TENG can be very useful for the development of intelligent laboratory systems.

## CONCLUSIONS

In summary, a dripping channel based liquid triboelectric nanogenerator (L-TENG) for droplet energy harvesting and sensing is demonstrated. The L-TENG is designed as a hybrid of a grating-electrode L-TENG and a single-electrode L-TENG, which are for energy harvesting and sensing, respectively. The inclination angle is optimized for single unfolded electrode panels. A folding design is adopted for improving the output density of the L-TENG. The maximum energy density of the folded 0.4 m L-TENG is 7.1% higher than that of the unfolded case, and the enhancement is 141.18% for the folded 0.6 m L-TENG. A typical setup in chemistry is demonstrated. When

dripping from a funnel, the energy of droplets can be successively harvested and stored. Moreover, the droplet interval, the count of the droplets, and the total duration of dripping can also be sensed by the dripping channel. Such automatically obtained information can show the degree of the dripping and help to estimate the progress of the chemical reaction. The device can be very useful for the development of intelligent laboratory systems and can also contribute to the optimization of the L-TENGs for harvesting droplet energy.

## EXPERIMENTAL SECTION

**Fabrication of the Electrode Panel.** First, epoxy glass fiber boards plated with a layer of electrodes were fabricated by printed circuit board (PCB) manufacturing technology. The boards have the same widths of 12 cm and thicknesses of 1.6 mm, while the lengths are 0.2 m, 0.4 m, and 0.6 m, respectively, for different devices. A pair of copper electrodes with an interdigital pattern (35  $\mu\text{m}$  in thickness) were plated on the epoxy glass fiber substrate, and each finger has a dimension of 8 mm  $\times$  98 mm with an interval of 2 mm. The electrodes were covered with a thin layer of gold to prohibit oxidation. A steel rod with a diameter of 1 mm and a length of 88 mm was installed at the end of the board, and a 0.3 mm thick aluminum sheet was placed under the steel bar for fixing and conducting. A PTFE film (80  $\mu\text{m}$  in thickness) was adhered on the board and the steel rod as a triboelectric layer.

**Fabrication of the L-TENG.** Electrode panels with a length of 0.2 m were fixed on an acrylic stand with a folded configuration. The total height of the folded structure is 18 cm. For the 0.4 m L-TENG, two electrode panels were fixed with the same inclination angle. For the 0.6 m L-TENG, three electrode panels were used. A vertical gap of about 10.78 mm between adjacent panels was introduced by displacing the panels horizontally.

**Characterization.** The transferred charges, current, and voltage were characterized by an electrometer (Keithley 6514). The liquid in the funnel was grounded in the experiment. The raw output signals (except the data of charging the capacitor) were band-block filtered from 49 to 51 Hz after the experiments to remove the noise in the environment.

## ASSOCIATED CONTENT

### Supporting Information

The Supporting Information is available free of charge at <https://pubs.acs.org/doi/10.1021/acsnano.0c04413>.

Figures S1–S5: SEM image of the PTFE surface; basic characterization of the unfolded grating-electrode L-TENGs tested with a motor; electrode connections of different segments in the folded 0.4 and 0.6 m grating-electrode L-TENGs; basic characterization of the folded grating-electrode L-TENGs tested with a motor; and basic characterization of the folded grating-electrode L-TENGs tested with a funnel (PDF)

Video S1: The process of droplets dripping from the funnel through the dripping channel (MP4)

Video S2: Sensing process of the dripping channel (MP4)

## AUTHOR INFORMATION

### Corresponding Author

**Zhong Lin Wang** – CAS Center for Excellence in Nanoscience, Beijing Key Laboratory of Micro-nano Energy and Sensor, Beijing Institute of Nanoenergy and Nanosystems, Chinese Academy of Sciences, Beijing 100083, P. R. China; School of Nanoscience and Technology, University of Chinese Academy of Sciences, Beijing 100049, P. R. China; School of Materials Science and Engineering, Georgia Institute of Technology, Atlanta, Georgia 30332, United States; [orcid.org/0000-0002-5530-0380](https://orcid.org/0000-0002-5530-0380); Email: [zhong.wang@mse.gatech.edu](mailto:zhong.wang@mse.gatech.edu)

## Authors

**Wei Zhong** – CAS Center for Excellence in Nanoscience, Beijing Key Laboratory of Micro-nano Energy and Sensor, Beijing Institute of Nanoenergy and Nanosystems, Chinese Academy of Sciences, Beijing 100083, P. R. China; School of Nanoscience and Technology, University of Chinese Academy of Sciences, Beijing 100049, P. R. China

**Liang Xu** – CAS Center for Excellence in Nanoscience, Beijing Key Laboratory of Micro-nano Energy and Sensor, Beijing Institute of Nanoenergy and Nanosystems, Chinese Academy of Sciences, Beijing 100083, P. R. China; School of Nanoscience and Technology, University of Chinese Academy of Sciences, Beijing 100049, P. R. China

**Fei Zhan** – CAS Center for Excellence in Nanoscience, Beijing Key Laboratory of Micro-nano Energy and Sensor, Beijing Institute of Nanoenergy and Nanosystems, Chinese Academy of Sciences, Beijing 100083, P. R. China; School of Nanoscience and Technology, University of Chinese Academy of Sciences, Beijing 100049, P. R. China

**Haiming Wang** – CAS Center for Excellence in Nanoscience, Beijing Key Laboratory of Micro-nano Energy and Sensor, Beijing Institute of Nanoenergy and Nanosystems, Chinese Academy of Sciences, Beijing 100083, P. R. China; School of Nanoscience and Technology, University of Chinese Academy of Sciences, Beijing 100049, P. R. China

**Fan Wang** – CAS Center for Excellence in Nanoscience, Beijing Key Laboratory of Micro-nano Energy and Sensor, Beijing Institute of Nanoenergy and Nanosystems, Chinese Academy of Sciences, Beijing 100083, P. R. China; School of Nanoscience and Technology, University of Chinese Academy of Sciences, Beijing 100049, P. R. China

Complete contact information is available at:

<https://pubs.acs.org/doi/10.1021/acsnano.0c04413>

## Author Contributions

<sup>#</sup>W. Zhong and L. Xu contributed equally to this work.

## Notes

The authors declare no competing financial interest.

## ACKNOWLEDGMENTS

The research was supported by the National Key R & D Project from Minister of Science and Technology, China (2016YFA0202704), National Natural Science Foundation of China (Grant Nos. 51735001 and 51432005), and Beijing Municipal Science and Technology Commission (Grant Nos. Z171100002017017 and Y3993113DF).

## REFERENCES

- (1) Pang, X.; Zhao, H.; Ma, S. A Microfluidics Reaction System with Automation for a Multicomponent Reaction. *Adv. Intell. Syst.* **2020**, *2*, 1900191.
- (2) Fan, F.-R.; Tian, Z.-Q.; Wang, Z. L. Flexible Triboelectric Generator. *Nano Energy* **2012**, *1*, 328–334.
- (3) Wang, Z. L. On Maxwell's Displacement Current for Energy and Sensors: The Origin of Nanogenerators. *Mater. Today* **2017**, *20*, 74–82.
- (4) Niu, S.; Wang, Z. L. Theoretical Systems of Triboelectric Nanogenerators. *Nano Energy* **2015**, *14*, 161–192.
- (5) Wang, Z. L.; Chen, J.; Lin, L. Progress in Triboelectric Nanogenerators as a New Energy Technology and Self-Powered Sensors. *Energy Environ. Sci.* **2015**, *8*, 2250–2282.
- (6) Wang, Z. L.; Jiang, T.; Xu, L. Toward the Blue Energy Dream by Triboelectric Nanogenerator Networks. *Nano Energy* **2017**, *39*, 9–23.
- (7) Zi, Y.; Guo, H.; Wen, Z.; Yeh, M.-H.; Hu, C.; Wang, Z. L. Harvesting Low-Frequency (<5 Hz) Irregular Mechanical Energy: A

Possible Killer Application of Triboelectric Nanogenerator. *ACS Nano* **2016**, *10*, 4797–4805.

(8) Zhao, J.; Zhen, G.; Liu, G.; Bu, T.; Liu, W.; Fu, X.; Zhang, P.; Zhang, C.; Wang, Z. L. Remarkable Merits of Triboelectric Nanogenerator than Electromagnetic Generator for Harvesting Small-Amplitude Mechanical Energy. *Nano Energy* **2019**, *61*, 111–118.

(9) Tang, W.; Chen, B. D.; Wang, Z. L. Recent Progress in Power Generation from Water/Liquid Droplet Interaction with Solid Surfaces. *Adv. Funct. Mater.* **2019**, *29*, 1901069.

(10) Lin, S.; Xu, L.; Chi Wang, A.; Wang, Z. L. Quantifying Electron-Transfer in Liquid-Solid Contact Electrification and the Formation of Electric Double-Layer. *Nat. Commun.* **2020**, *11*, 399.

(11) Nie, J.; Ren, Z.; Xu, L.; Lin, S.; Zhan, F.; Chen, X.; Wang, Z. L. Probing Contact-Electrification-Induced Electron and Ion Transfers at a Liquid–Solid Interface. *Adv. Mater.* **2020**, *32*, 1905696.

(12) Lin, Z. H.; Cheng, G.; Lin, L.; Lee, S.; Wang, Z. L. Water-Solid Surface Contact Electrification and Its Use for Harvesting Liquid-Wave Energy. *Angew. Chem., Int. Ed.* **2013**, *52*, 12545–12549.

(13) Lin, Z.-H.; Cheng, G.; Wu, W.; Pradel, K. C.; Wang, Z. L. Dual-Mode Triboelectric Nanogenerator for Harvesting Water Energy and as a Self-Powered Ethanol Nanosensor. *ACS Nano* **2014**, *8*, 6440–6448.

(14) Lin, Z.-H.; Cheng, G.; Lee, S.; Pradel, K. C.; Wang, Z. L. Harvesting Water Drop Energy by a Sequential Contact-Electrification and Electrostatic-Induction Process. *Adv. Mater.* **2014**, *26*, 4690–4696.

(15) Zhao, X. J.; Kuang, S. Y.; Wang, Z. L.; Zhu, G. Highly Adaptive Solid-Liquid Interfacing Triboelectric Nanogenerator for Harvesting Diverse Water Wave Energy. *ACS Nano* **2018**, *12*, 4280–4285.

(16) Xu, M.; Wang, S.; Zhang, S. L.; Ding, W.; Kien, P. T.; Wang, C.; Li, Z.; Pan, X.; Wang, Z. L. A Highly-Sensitive Wave Sensor Based on Liquid-Solid Interfacing Triboelectric Nanogenerator for Smart Marine Equipment. *Nano Energy* **2019**, *57*, 574–580.

(17) Zheng, L.; Cheng, G.; Chen, J.; Lin, L.; Wang, J.; Liu, Y.; Li, H.; Wang, Z. L. A Hybridized Power Panel to Simultaneously Generate Electricity from Sunlight, Raindrops, and Wind around the Clock. *Adv. Energy Mater.* **2015**, *5*, 1501152.

(18) Pan, L.; Wang, J.; Wang, P.; Gao, R.; Wang, Y.-C.; Zhang, X.; Zou, J.-J.; Wang, Z. L. Liquid-FEP-Based U-Tube Triboelectric Nanogenerator for Harvesting Water-Wave Energy. *Nano Res.* **2018**, *11*, 4062–4073.

(19) Zhang, X.; Yu, M.; Ma, Z.; Ouyang, H.; Zou, Y.; Zhang, S. L.; Niu, H.; Pan, X.; Xu, M.; Li, Z.; Wang, Z. L. Self-Powered Distributed Water Level Sensors Based on Liquid–Solid Triboelectric Nanogenerators for Ship Draft Detecting. *Adv. Funct. Mater.* **2019**, *29*, 1900327.

(20) Zhu, H. R.; Tang, W.; Gao, C. Z.; Han, Y.; Li, T.; Cao, X.; Wang, Z. L. Self-Powered Metal Surface Anti-Corrosion Protection Using Energy Harvested from Rain Drops and Wind. *Nano Energy* **2015**, *14*, 193–200.

(21) Zheng, L.; Lin, Z.-H.; Cheng, G.; Wu, W.; Wen, X.; Lee, S.; Wang, Z. L. Silicon-Based Hybrid Cell for Harvesting Solar Energy and Raindrop Electrostatic Energy. *Nano Energy* **2014**, *9*, 291–300.

(22) Li, X.; Yeh, M.-H.; Lin, Z.-H.; Guo, H.; Yang, P.-K.; Wang, J.; Wang, S.; Yu, R.; Zhang, T.; Wang, Z. L. Self-Powered Triboelectric Nanosensor for Microfluidics and Cavity-Confined Solution Chemistry. *ACS Nano* **2015**, *9*, 11056–11063.

(23) Chen, J.; Guo, H.; Zheng, J.; Huang, Y.; Liu, G.; Hu, C.; Wang, Z. L. Self-Powered Triboelectric Micro Liquid/Gas Flow Sensor for Microfluidics. *ACS Nano* **2016**, *10*, 8104–8112.

(24) Cheng, X.; Miao, L.; Chen, H.; Song, Y.; Su, Z.; Chen, X.; Wang, H.; Zhang, M.; Zhang, H. Triboelectrification Based Active Sensor for Liquid Flow and Bubble Detecting. *2017 IEEE 30th International Conference on Micro Electro Mechanical Systems (MEMS)*, Las Vegas, 22–26 Jan. 2017; IEEE: Piscataway, 2017; pp 845–848.

(25) Niu, S.; Wang, S.; Liu, Y.; Zhou, Y. S.; Lin, L.; Hu, Y.; Pradel, K. C.; Wang, Z. L. A Theoretical Study of Grating Structured Triboelectric Nanogenerators. *Energy Environ. Sci.* **2014**, *7*, 2339–2349.

(26) Lin, Z.-H.; Cheng, G.; Li, X.; Yang, P.-K.; Wen, X.; Wang, Z. L. A Multi-Layered Interdigitative-Electrodes-Based Triboelectric Nanogenerator for Harvesting Hydropower. *Nano Energy* **2015**, *15*, 256–265.

(27) Kil Yun, B.; Soo Kim, H.; Joon Ko, Y.; Murillo, G.; Hoon Jung, J. Interdigital Electrode Based Triboelectric Nanogenerator for Effective Energy Harvesting from Water. *Nano Energy* **2017**, *36*, 233–240.

(28) He, C.; Chen, B. D.; Jiang, T.; Xu, L.; Han, C. B.; Gu, G. Q.; Wang, Z. L. Radial-Grating Pendulum-Structured Triboelectric Nanogenerator for Energy Harvesting and Tilting-Angle Sensing. *Adv. Mater. Technol.* **2018**, *3*, 1700251.

(29) Xie, Y.; Wang, S.; Niu, S.; Lin, L.; Jing, Q.; Yang, J.; Wu, Z.; Wang, Z. L. Grating-Structured Freestanding Triboelectric-Layer Nanogenerator for Harvesting Mechanical Energy at 85% Total Conversion Efficiency. *Adv. Mater.* **2014**, *26*, 6599–6607.

(30) Xu, L.; Pang, Y. K.; Zhang, C.; Jiang, T.; Chen, X. Y.; Luo, J. J.; Tang, W.; Cao, X.; Wang, Z. L. Integrated Triboelectric Nanogenerator Array Based on Air-Driven Membrane Structures for Water Wave Energy Harvesting. *Nano Energy* **2017**, *31*, 351–358.

(31) Zhong, W.; Xu, L.; Yang, X.; Tang, W.; Shao, J.; Chen, B.; Wang, Z. L. Open-Book-Like Triboelectric Nanogenerators Based on Low-Frequency Roll-Swing Oscillators for Wave Energy Harvesting. *Nanoscale* **2019**, *11*, 7199–7208.

(32) Xiao, T. X.; Liang, X.; Jiang, T.; Xu, L.; Shao, J. J.; Nie, J. H.; Bai, Y.; Zhong, W.; Wang, Z. L. Spherical Triboelectric Nanogenerators Based on Spring-Assisted Multilayered Structure for Efficient Water Wave Energy Harvesting. *Adv. Funct. Mater.* **2018**, *28*, 1802634.

(33) An, J.; Wang, Z. M.; Jiang, T.; Liang, X.; Wang, Z. L. Whirling-Folded Triboelectric Nanogenerator with High Average Power for Water Wave Energy Harvesting. *Adv. Funct. Mater.* **2019**, *29*, 1904867.

(34) Yang, P. K.; Lin, Z. H.; Pradel, K. C.; Lin, L.; Li, X.; Wen, X.; He, J. H.; Wang, Z. L. Paper-Based Origami Triboelectric Nanogenerators and Self-Powered Pressure Sensors. *ACS Nano* **2015**, *9*, 901–907.

(35) Xia, K.; Zhang, H.; Zhu, Z.; Xu, Z. Folding Triboelectric Nanogenerator on Paper Based on Conductive Ink and Teflon Tape. *Sens. Actuators, A* **2018**, *272*, 28–32.

(36) Ren, Z.; Nie, J.; Xu, L.; Jiang, T.; Chen, B.; Chen, X.; Wang, Z. L. Directly Visualizing Tactile Perception and Ultrasensitive Tactile Sensors by Utilizing Body-Enhanced Induction of Ambient Electromagnetic Waves. *Adv. Funct. Mater.* **2018**, *28*, 1805277.